Clim Dyn (2018) 50:289–301
DOI 10.1007/s00382-017-3607-z

Comparison of Arctic sea ice thickness and snow depth estimates from CFSR with in situ observations

Kazutoshi Sato[1] · **Jun Inoue**[1,2,3]

Received: 29 August 2016 / Accepted: 26 February 2017 / Published online: 11 March 2017

Abstract Sea ice growth is modulated by snow cover, and understanding this relationship requires an accurate determination of snow depth. However, a lack of in situ measurements complicates understanding of the interaction of snow depth with sea ice growth. We evaluated the accuracy of Climate Forecast System Reanalysis (CFSR) data for snow depth and sea ice thickness to study the change of snow depth on Arctic sea ice. We compared CFSR and snow depth data from 35 drifting buoys in 2002–2013. The mean annual cycle of CFSR snow depth corresponded well with the buoy data. However, the CFSR data had a positive bias during winter (10–20 cm) and spring (5–25 cm), and a negative bias during summer (−25–0 cm) and autumn (−5–10 cm). The CFSR data showed increases in snow depth from 1979 to 2013 over the Beaufort and northern Chukchi Seas during November. Significant positive trends in precipitation contributed to increased snow depth in this region when sea ice began to form. The results of model experiments using a 1-D thermodynamic sea ice model in the CFSR demonstrated a recommended value of snow thermal conductivity (0.16 W m^{-1} K^{-1}), and suggested that the sea ice growth was effectively restricted by the recent increase in snow depth on thin ice during winter.

Keywords Snow depth · Sea ice · CFSR · Drifting buoy

✉ Kazutoshi Sato
sato.kazutoshi@nipr.ac.jp

[1] National Institute of Polar Research, Tachikawa, Tokyo, Japan

[2] The Graduate University for Advanced Studies, Tachikawa, Tokyo, Japan

[3] Japan Agency for Marine-Earth Science and Technology, Yokohama, Kanagawa, Japan

1 Introduction

Changes in snow properties (e.g., snow depth, snow cover, date of snowmelt, and surface albedo) influence atmospheric circulation patterns and surface heat budgets (Matsumura et al. 2010). Snow with a high surface albedo reflects downward solar radiation, which is important to those heat budgets. Previous studies have reported that the growth and decay of sea ice are controlled by snow loading (snow depth and density) on sea ice (Sturm et al. 2002; Blazey et al. 2013; Riche and Schneebeli 2013). Snow depth on sea ice is an important component of sea ice growth through the insulating effect of snow (Maykut and Untersteiner 1971). Increased snowfall on sea ice not only delays sea ice melt via reduced absorption of solar radiation but also prevents that ice from growing during autumn and winter. The climatology of snow depth for multiyear ice (MYI) has been generated using snow depth and density data from Soviet drifting stations in the Arctic Ocean since 1937 (Warren et al. 1999).

The drastic decline of Arctic sea ice (Stroeve et al. 2012; Comiso 2012) has led to ocean heating because of more absorption of solar radiation in recent decades, promoting additional sea ice melting (Perovich et al. 2007; Steele et al. 2010). Accelerated Arctic ice export through the Fram Strait also has caused MYI to be replaced by first-year ice (FYI) in recent decades (Maslanik et al. 2007, 2011). The IceBridge snow radar showed that spring snow depth on FYI was thinner than on MYI (Kurtz and Farrell 2011; Kwok et al. 2011). Abnormal heat storage in the ocean during summer reduces the recovery of sea ice and delays sea ice freeze-up during autumn and winter (Markus et al. 2009; Maslanik et al. 2011). In the subsequent spring, a decrease in snow depth is induced by a lack of autumn sea ice (Webster et al.

2014), and this is expected to continue in future scenarios (Hezel et al. 2012).

Heavy snowfall during recent winters associated with increased precipitation over Siberia and Europe was induced by an enhanced moisture source caused by sea ice retreat (Deser et al. 2010; Liu et al. 2012). Using an atmosphere–ocean coupled model, Krasting et al. (2013) suggested that an increase in total precipitation had contributed to a positive snowfall trend in winter at high latitudes during the twenty-first century. Changes in precipitation depend on the frequency and intensity of cyclones (Stroeve et al. 2011), indicating that a poleward shift of cyclone tracks may lead not only to cold winters in mid-latitudes but also to increased snowfall in the central Arctic (Inoue et al. 2012; Sato et al. 2014). The distribution of spring snow depths were assessed by Webster et al. (2014). However, previous studies have not been able to accurately describe changes in snow depth on Arctic sea ice during winter. Sea ice growth is reduced as ice thickness increases. Change in snow depth has a relatively strong impact on the growth rate of FYI compared to MYI (Maykut and Untersteiner 1971), so it is important to investigate how that change affects sea ice during winter.

The variation in snow depth on the ice has been unclear over recent decades, and the causes of the variation are poorly understood. Ice Mass Balance (IMB) buoys were deployed near the North Pole by the Cold Region Research and Engineering Laboratory (CRREL) in 1993, and drifted through the Fram Strait to the Greenland Sea. Some IMB buoys drifted to the Beaufort Sea (Perovich et al. 2017). Although in situ observation is limited in the area, models and satellites permit some determination of snow depth distribution on Arctic sea ice. However, there are discrepancies between observed and simulated snow depth which may be accounted for by surface roughness and other conditions (e.g., blowing snow and melt ponds). Blazey et al. (2013) simulated the distributions of snow depth and snow density in the Arctic using the Community Climate System Model (CCSM). A comparison of snow depth on sea ice demonstrated that CCSM-estimated snow depths were too thick, particularly over the Canadian Arctic Archipelago. The aim of the present study was to evaluate simulated snow depth and sea ice thickness in the National Centers for Environmental Prediction (NCEP) CFSR using IMB buoy observation data, and to investigate the change of snow depth on sea ice and its mechanisms from autumn to winter. In addition, various experiments were run with a 1-D thermodynamic model to investigate the influence of snow depth variation and surface forcing on ice growth. This model is used in the CFSR, and includes two equal layers of sea ice and one layer of snow.

2 Materials and methods

IMB buoys are operated on drifting MYI in the North Pole by the CRREL (Perovich et al. 2017). They have been deployed since 1993 and typically send data for 6 months to 1 year to monitor sea ice thickness, snow depth, and ice and surface temperatures. Data are open access and can be obtained from http://www.imb-crrel-dartmouth.org/imb.crrel. IMB buoys are set up on sea ice every spring and autumn. However, some buoys fail to obtain data during the melting season. In addition, the time resolution of the data from buoys before 2001 is not sufficient to resolve daily changes in snow depth. Although the Russian North Pole camp measured snow depth once a month or every 10 days during the years 1954–1991, the intervals between snow measurements makes it difficult to assess the reproducibility of snow depth in CFSR during these years. We selected 35 IMB buoys that measured snow depth and sea ice thickness several times a day, and used these measurements to investigate seasonal cycles (Fig. 1; Table 1). There are three main buoy regions: (1) around the North Pole, (2) from the Transpolar Drift Stream to the Fram Strait, and (3) Beaufort Gyre.

To further estimate seasonal changes of snow depth and sea ice thickness in the CFSR, we also used snow depth and sea ice thickness calculated from Ice, Cloud, and land Elevation Satellite (ICESat) and CryoSAT-2

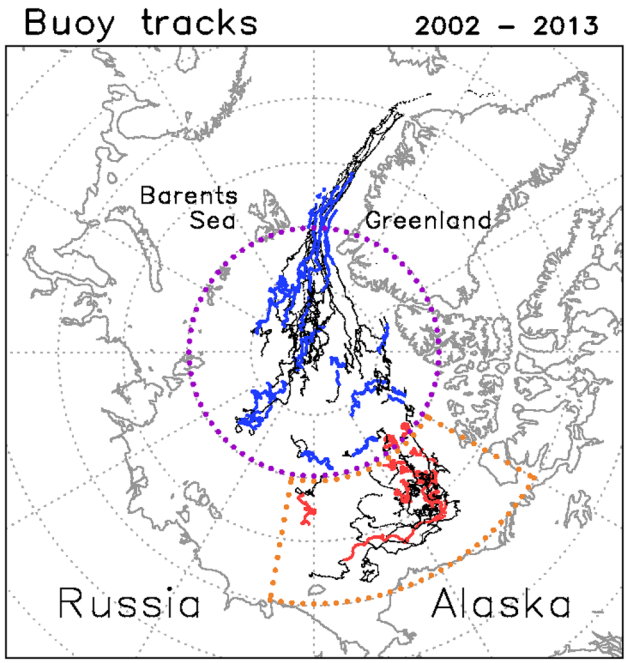

Fig. 1 All trajectories for IMB buoys over 2002–2013 (*black* and *colored lines*). Tracks during October to December are highlighted by *red* (Beaufort Sea) and *blue* (North Pole)

Table 1 A list of Ice Mass Balance buoys (IMBs) used in this study (years of deployments, availability of the data, and regions)

Buoy	Snow	Ice	Area
2002A*	○	○	North Pole
2003C	○		Beaufort Sea
2003D	○	○	Beaufort Sea
2004A*	○	○	North Pole
2004B*	○	○	North Pole
2004C	○	○	North Pole
2004D	○	○	North Pole
2004E*	○	○	North Pole
2005F	○	○	North Pole
2006B	○		North Pole
2006C	○		Beaufort Sea
2006D*	○	○	North Pole
2006E*	○	○	North Pole
2007C	○	○	North Pole
2007H		○	North Pole
2007J		○	North Pole
2008B		○	North Pole
2008C		○	North Pole
2008D	○	○	North Pole
2009F	○		Beaufort Sea
2010A	○	○	North Pole
2010E	○	○	Beaufort Sea
2010F	○	○	Beaufort Sea
2010H	○	○	Beaufort Sea
2011I	○	○	Beaufort Sea
2011J	○	○	Beaufort Sea
2011K	○	○	Beaufort Sea
2011M	○	○	North Pole
2012B		○	North Pole
2012D	○	○	North Pole
2012H*	○	○	Beaufort Sea
2012I*	○	○	Beaufort Sea
2012J	○	○	North Pole
2012L*	○	○	Beaufort Sea
2013B	○	○	North Pole

*IMBs which were used in Fig. 5

satellite data sets. The ICESat, launched in January 2003 (Kwok et al. 2004), performed campaigns during 2003 and 2008 (Kwok and Cunningham 2008). The data obtained from 15 campaigns were used in this study. Data are available at https://nsidc.org. The CryoSat-2, launched in November 2010, measures freeboard and ice thickness from October through April every year (Laxon et al. 2013). The CryoSat-2 sea ice thickness and snow depth data are available from http://www.meereisportal.de (Ricker et al. 2014). The procedure of data processing is summarized in the "Appendix".

The CFSR data are provided on a 0.5° × 0.5° latitude/longitude grid and are produced by the NCEP (Saha et al. 2010). We used 6-hourly CFSR data from January 1979 to March 2011. After April 2011, the CFS Version 2 (CFSv2) was used (Saha et al. 2014). These data included meteorological (air temperature, specific humidity, wind speed, sea level pressure, precipitation and evaporation) and oceanographic (sea surface temperature, snow depth, sea ice thickness and sea ice concentration) parameters. The snow depth and ice thickness from the IMBs were not assimilated in the CFSR. We calculated a weighted average of snow depth using four grid points close to buoy positions and compared these with observation data.

The Geophysical Fluid Dynamics Laboratory sea ice simulator, which has two layers of ice and one layer of snow, is used in CFSR. We ran a 1-D model with three layers to estimate the impact of snow and sea ice thermodynamics on ice–ice growth. Snow and ice mass changes were estimated from the energy balance at the top and bottom surfaces. The surface energy flux is defined as follows:

$$M_s = K_u(dT/dz)_u - F_a, \quad (1)$$

$$F_a = F_{LW} + F_{SW} + F_{SH} + F_{LH}, \quad (2)$$

where F_a is surface energy budget, K_u is effective conductive coupling of snow-ice layer as a function of ice thickness and snow depth defined by Winton (1999), $(dT/dz)_u$ is the temperature gradient between surface and upper ice temperature, F_{LW} is net longwave radiation, F_{SW} is net shortwave radiation, F_{SH} is the surface sensible heat flux, and F_{LH} is the surface latent heat flux. The period of the model run was from 16 September to 31 May the subsequent year. The model was initialized with observed mean ice thickness. Surface heat forcing (longwave and shortwave radiation, turbulent heat flux, and surface temperature) was derived from the CFSR. Although turbulent heat and radiative fluxes depend on parameterizations, those in the CFSR are close to observations with small biases (Lindsay et al. 2014). Therefore, we used the sum of turbulent heat fluxes, longwave and shortwave radiation for the surface heat budget. When the surface energy budget is positive (upward), ice thickness (H_i) is increased by:

$$dH_i = (M_s\Delta t - Lh_s) / E, \quad (3)$$

where L is the latent heat of freezing and E is the enthalpy of sea ice. Snow depths (h_s) are derived from IMB buoys. At the bottom of the ice, the energy flux is given by:

$$M_b = F_b - F_c, \quad (4)$$

$$F_c = K_{bice}(dT/dz)_{b,} \quad (5)$$

where F_b is oceanic heat flux, $(dT/dz)_b$ is the temperature gradient between lower ice and ocean temperature, and K_{bice} is conductivity of the lower ice. When M_b is negative,

there is bottom freezing at the ice–ocean interface. The ice thickness is increased by:

$$dH_i = M_b \Delta t/(C + L), \quad (6)$$

where C is the ice heat capacity. Details of this model are described in Winton (1999). In our study, we focused on the thermodynamic processes of sea ice, because that model does not consider dynamic processes such as ice motion.

3 Results and discussion

3.1 Snow depth on sea ice

3.1.1 Comparison between IMB buoy and CFSR data

The results from Warren et al. (1999) based on the Russian North Pole drifting data showed that snow depth was at a local maximum in spring and local minimum in summer, with regional differences. Blazey et al. (2013) indicated that the distribution of simulated snow depth bias in the CCSM had a regional difference across the Arctic. Therefore, we evaluated the performance of snow depth in the CFSR by comparison with data from 35 IMB buoys in different areas (Beaufort Sea and North Pole). Mean seasonal cycles of monthly snow depth from observations and the CFSR in each area are shown in Fig. 2a, b. Red and blue lines show monthly average snow depths observed by IMB buoys in the Beaufort Sea (red lines in Fig. 1) and North Pole (blue lines in Fig. 1), respectively. Black lines show weighted average values at four grid points of the CFSR, near buoy locations.

In the Beaufort Sea region, the seasonal cycle of snow depth in the CFSR was reproduced well, although there were biases during summer to autumn (5 cm) and winter to spring (10 cm). In the North Pole region, biases were larger than in the Beaufort Sea, particularly from winter to spring (>15 cm in March and April). Snow depth was nearly zero in July, despite some depth from the observations (10 cm). The early snowmelt in the CFSR during June may explain this difference. An additional aspect of the modeled snow depth is that the difference between the CFSR and observations became larger from autumn to winter, in both regions. Although the CFSR snow depth increased from November to January, the IMB observed a decrease in snow depth. According to Serreze et al. (2012), the CFSR has large positive humidity biases during December and January compared with radiosonde observations, which may partly cause positive snowfall biases on sea ice. Furthermore, the CFSR does not consider snow densification on sea ice (CFSR team, personal communication), resulting in further biases during December (Fig. 2a, b).

The correlation coefficients of snow depth between in situ measurements and CFSR (Fig. 2c) and associated scatter plots (Fig. 2d–g) indicated that the highest correlation was in November (>0.65) with little bias. December had relatively high correlations (>0.50). In contrast, there were weak correlations (<0.50) for the other months except for the Beaufort Sea for August. The CFSR snow depth during September was smaller than that for IMBs where observed snow depth exceeded 20 cm (Fig. 2d). The opposite was found during December (Fig. 2g).

3.1.2 Change in snow depth on sea ice in CFSR

Because the differences in snow depth between CFSR and IMBs over the Beaufort Sea were smaller than over the North Pole (Fig. 2a, b), we focused on horizontal change in snow depth during October and November when the Beaufort Sea had a relatively high correlation coefficient (Fig. 2c). To investigate horizontal changes in snow depth on the sea ice and their causes (e.g., changes in precipitation, temperature and timing of sea ice formation), we used trends in snow depth and sea level pressure during October and November 1979–2013 across the entire Arctic Ocean (Fig. 3a, d). Negative trends in snow depth in October were found over the Barents and Beaufort Seas (Fig. 3a). Such decreases in snow depth were associated with a decline in precipitation over these regions (Fig. 3b). In contrast, a reduction in sea ice cover was related to a decrease in snow accumulation in other regions (Kara, Laptev, East Siberian and Chukchi Seas in Fig. 3c). Because the onset of sea ice freeze-up was delayed in these regions owing to sea ice reduction during October, snow fell directly into the ocean (Markus et al. 2009; Webster et al. 2014). An increase in precipitation across the Seas was mainly caused by invigorated synoptic activity, which was represented by 8-day, high-pass filtered eddy heat fluxes (v'T'), averaged between the 1000 and 850 hPa levels (Fig. 3b). In contrast, over the North Pole, a strengthened Beaufort high-pressure system (contours in Fig. 3a) was associated with decreased precipitation (Fig. 3b), reducing snow depth on the MYI. According to Maslanik et al. (2011), the fraction of the oldest sea ice types decreased in the Canadian Basin. Elsewhere in the Arctic, disappearing sea ice may have reduced the amount of snow surviving through the summer on MYI.

In November, there was a positive trend (more than 2 cm per decade) in snow depth over the northern Chukchi and Beaufort Seas (Fig. 3d). The cyclonic anomaly of sea level pressure was dominant in the Beaufort Gyre, enhancing precipitation over the northern Chukchi Sea (Fig. 3e). In contrast, over the Beaufort Sea, increased precipitation was found along the northern Alaska coast despite weakened synoptic activity. This result indicates that short-lived phenomena such as polar lows (Inoue et al. 2010) may

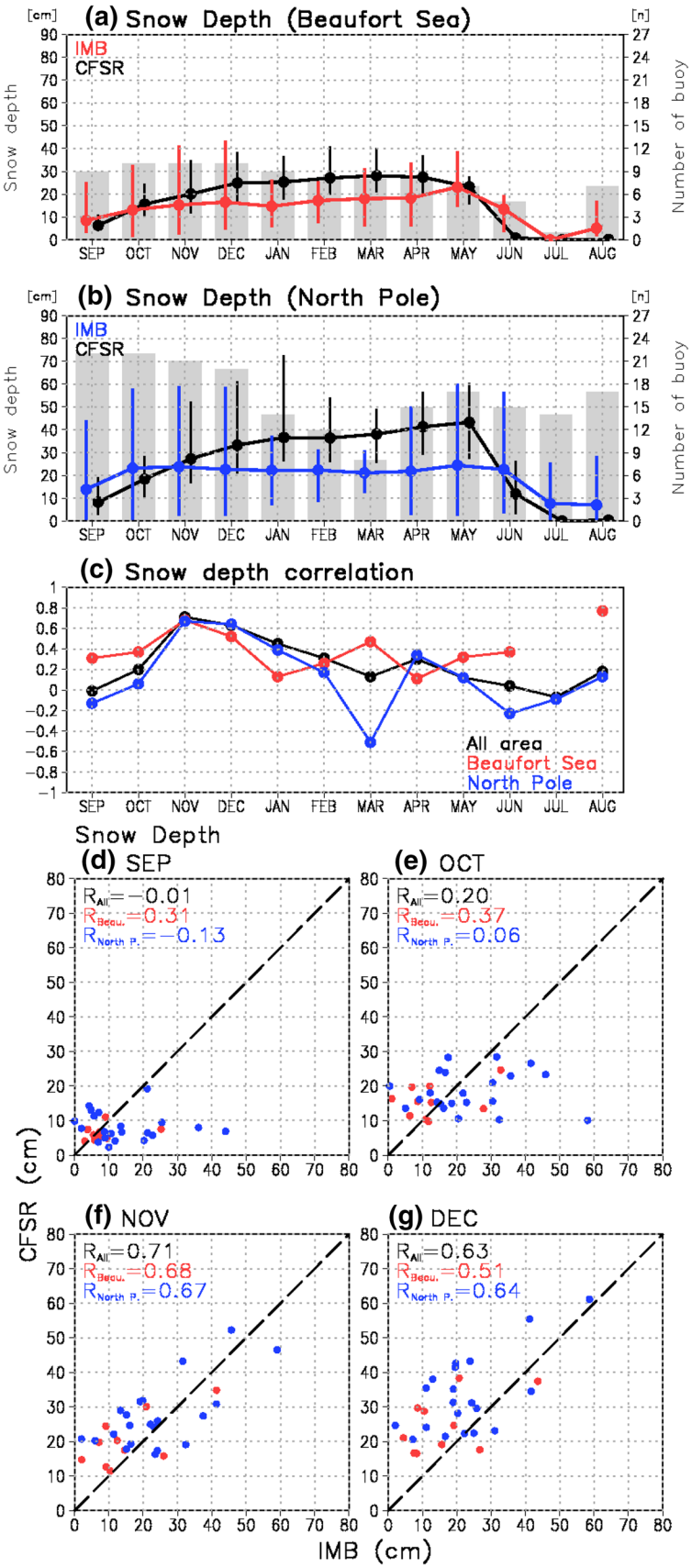

Fig. 2 **a** Monthly average snow depth on sea ice from CFSR (*black*) and IMB buoys (*red*) over the Beaufort Sea during 2002–2013. *Vertical lines* indicate ranges of snow depth in each month. *Gray bars* show number of buoy. **b** Same as (**a**), but for North Pole. **c** Monthly correlation coefficients of snow depth between CFSR and IMB over each region (*red* Beaufort Sea; *blue* North Pole; *black* all regions). The scatter plots of monthly averaged snow depth between IMB and CFSR for **d** September, **e** October, **f** November and **g** December during 2002–2013. *Color dots* indicate each region (*red* Beaufort Sea; *blue* North Pole)

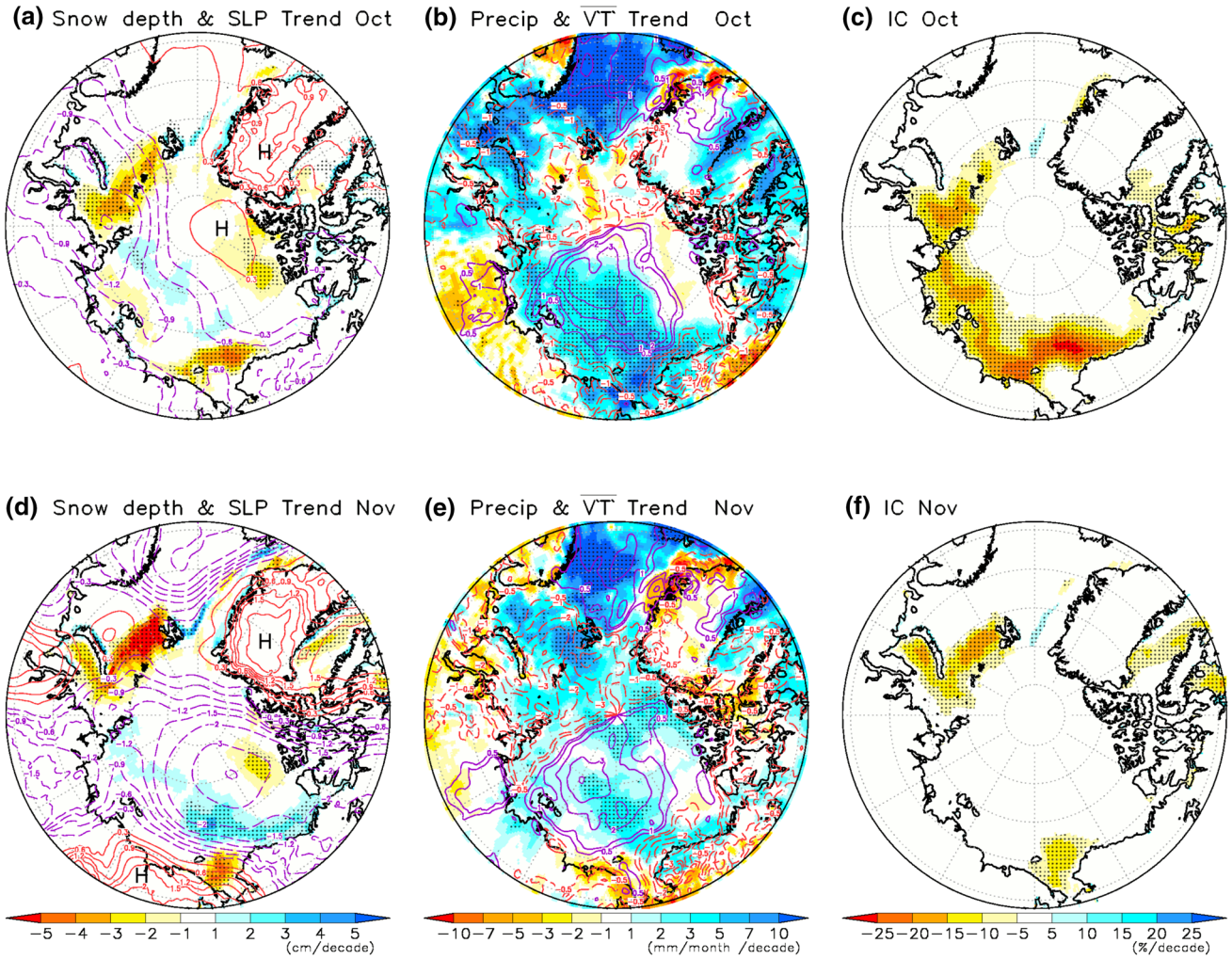

Fig. 3 Spatial maps of trends in **a** snow depth (*shaded* cm decade^{-1}) and sea level pressure (contour; hPa decade^{-1}) (1979–2013), **b** precipitation (*shading* mm month^{-1} decade^{-1}) and 8-day high-pass filtered poleward eddy heat flux averaged between 1000 and 850 hPa (contour; Km s^{-1}), and **c** ice cover (% decade^{-1}) in October. Same as (**a**), **b** and **c**, but for November in (**d**), (**e**) and (**f**). *Stippled areas* represent significant trends exceeding 95% confidence level for (**a, d**) snow depth (**b, e**) precipitation and (**c, f**) ice cover. H in (**a**) (**d**) shows the area of positive SLP trend

contribute to precipitation change. In addition, enhanced evaporation (i.e., latent heat flux) from extended ice-free areas caused increased precipitation over the Chukchi Sea (Kurita 2011). In contrast to the absence of sea ice in October, sea ice formation around the marginal ice zone allowed snow to accumulate (Fig. 3c, f). We found a positive trend in snow depth there, suggesting that the growth of thin FYI is sensitive to variations of snow depth (discussed later). Over the Barents and Kara Seas, however, the situation in which the sea ice reduction contributed to decreased snow accumulation was the same as in October (Fig. 3f).

Webster et al. (2014) suggested that the Arctic had relatively high precipitation during September and October, which would cause large changes in snow depth on sea ice. However, the relationship in snow depth between observations and CFSR seemed to be weak during these months. There was no positive trend in snow depth on sea ice because of large sea ice variability (not shown).

3.2 Sea ice thickness in CFSR

3.2.1 Comparison between IMB buoy and CFSR data

The same evaluation was done for sea ice thickness (Fig. 4). Observed thickness in the Beaufort Sea indicated a gradual increase from December through May, and a relatively rapid decrease from June through September (Fig. 4a). However, modeled ice thickness began to increase in

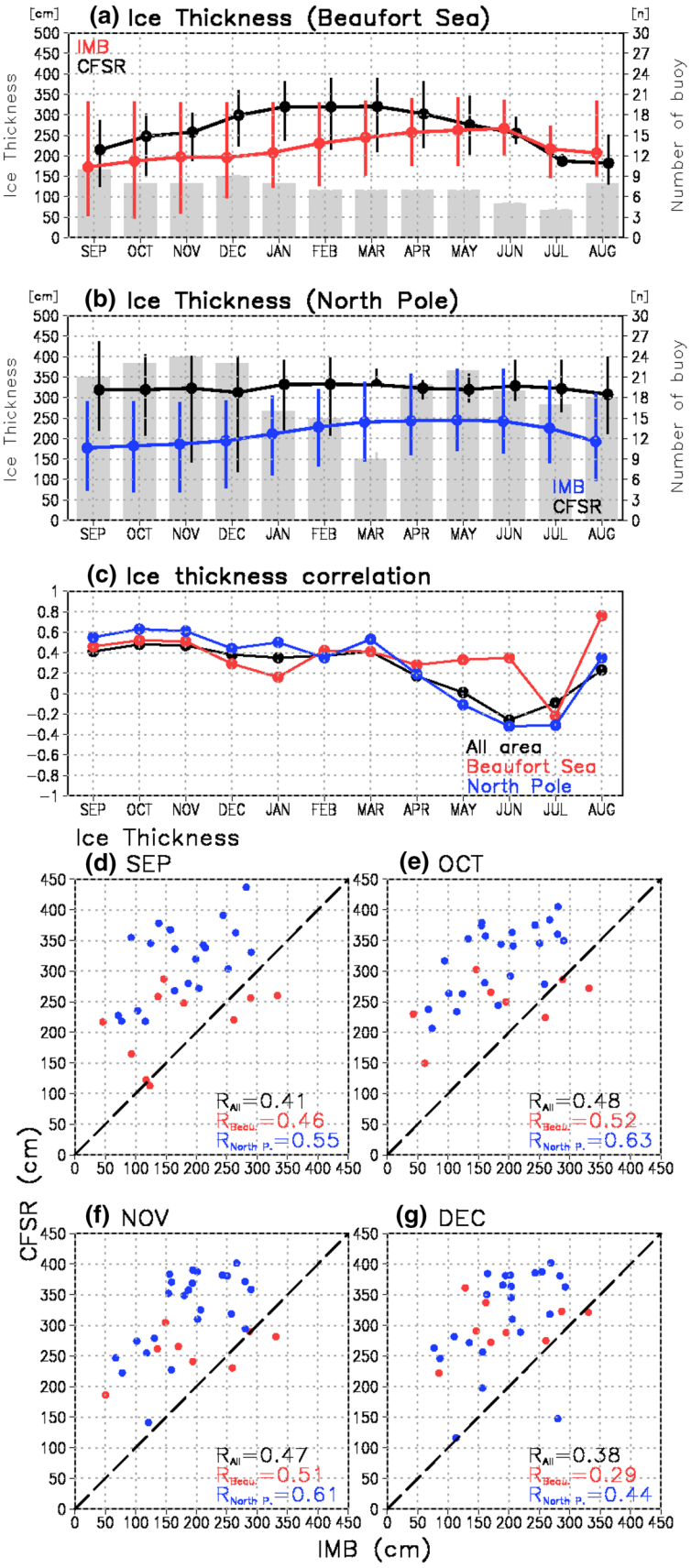

Fig. 4 **a** Monthly average sea ice thickness from CFSR (*black*) and IMB buoys (*red*) over the Beaufort Sea during 2002–2013. *Vertical lines* indicate ranges of sea ice thickness in each month. *Gray bars* show number of buoy. **b** Same as (**a**), but for North Pole. **c** Monthly correlation coefficients of sea ice thickness between CFSR and IMB over each region (*red* Beaufort Sea; *blue* North Pole; *black* all regions). The scatter plots of monthly averaged sea ice thickness between IMB and CFSR for **d** September, **e** October, **f** November and **g** December during 2002–2013. *Color dots* indicate each region (*red* Beaufort Sea; *blue* North Pole)

September and continued to increase until January, when there was a gradual decline from March through July. The seasonal cycle was not reproduced, showing large biases >1 m during winter, although those biases became smaller between May and August (<0.3 m). Sea ice thickness began to increase from autumn in the CFSR, but observed data showed that it did not grow until early winter. The causes of sea ice growth biases are discussed later.

CFSR ice thickness over the North Pole had a bias in all months, with greater differences during summer and winter (Fig. 4b). IMB data revealed that snowmelt coincided with decreased ice thickness during May to August, indicating ice melt at the bottom and surface of the ice. Over the Beaufort Sea, stronger melting at the bottom and surface produced smaller ice thickness biases in the CFSR during August and September. In contrast, in the North Pole, ice thickness biases were large during June and July, because of less predicted sea ice melt in the CFSR. These biases persisted and remained constant through autumn and winter. Sea ice thickness did not change much seasonally compared with observations, resulting in very substantial biases from summer through winter, although correlation coefficients of sea ice thickness over the North Pole exceeded 0.6 during October and November (Fig. 4c–f). Over the Beaufort Sea, the amplitude of seasonal changes of ice thickness in the CFSR was very large compared with observations. Therefore, there were weak correlations (<0.50) for the other months except for the Beaufort Sea for August.

3.2.2 *Sea ice thickness biases in CFSR*

Compared with the North Pole, snow and ice melt predictions were reproduced well over the Beaufort Sea. However, the time of ice growth during autumn was too early relative to observations, resulting in substantial growth during autumn and winter. Generally, sea ice thickness begins to increase in winter when the temperature of sea ice drops below the freezing temperature of seawater. To understand the differences in the timing and rate of ice growth during early summer, we assessed the impact of snow and ice parameterization on that growth using a 1-D thermodynamic model. To test the model's ability to simulate ice growth, we selected nine buoys that had sufficient data on both snow depth and ice thickness, and used observed snow depth for the model. Each model run was started on 16 September and run to 31 May the subsequent year, and was initialized with mean observed ice thickness. Oceanic heat flux was assumed to be zero.

The 1-D thermodynamic model followed observed ice thickness closely in both areas, and reproduced seasonal change in that thickness (Fig. 5, blue line). Sea ice in the model began to grow when temperature of that ice

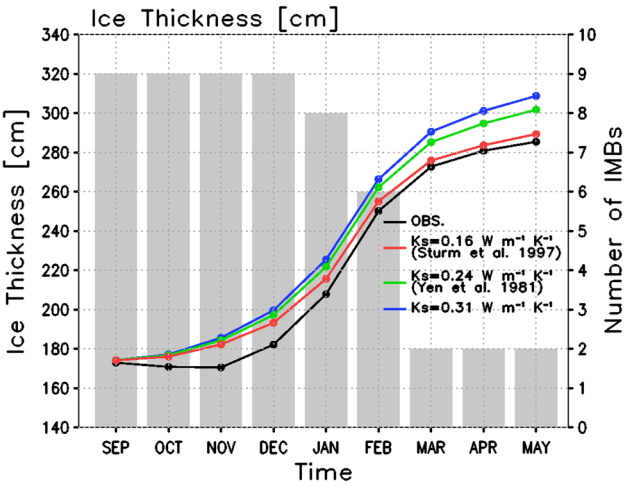

Fig. 5 Monthly average sea ice thickness from IMB buoys (*black*) and 1-D thermodynamic model-simulated ice thickness using different snow thermal conductivity. *Gray bars* show the number of observations

dropped below the freezing temperature of seawater. The modeled sea ice growth rate depended on sea ice temperature and energy from the bottom. Upper ice cooling began earlier than that of lower ice because of a time lag. Although upper ice cooling began during September, lower ice cooling began during November. Therefore, upper sea ice temperature influenced that of lower sea ice because of thermal energy transport, meaning that the former temperature was important in determining the timing of sea ice freezing and the ice growth rate.

However, the difference between the model and observations gradually increased from December through May, with biases >20 cm during May (Fig. 5, blue line). The transfer of heat from air–ice interactions depended on the thermal conductivity of snow. The high conductivity (0.31 W m^{-1} K^{-1}) used in the CFSR led to an overestimation of ice growth (Lecomte et al. 2013). To assess the effect of the snow thermal conductivity bias on the error in ice growth, the value 0.31 W m^{-1} K^{-1} and the two following parameterizations were tested:

$$K_s = K_i\left(\rho_s/\rho_w\right)^{1.88}, \tag{8}$$

$$K_s = 0.138 - 0.00101\,\rho_s + 0.000003233\,\rho_s^2, \tag{9}$$

where K_i (=2.03 W m^{-1} K^{-1}) is the thermal conductivity of ice, and ρ_s (330 kg m^{-3}) and ρ_w (1025 kg m^{-3}) are the densities of snow and freshwater. Parameterizations of Eqs. (8) and (9) correspond to Yen (1981) and Sturm et al. (1997). Ice thickness simulated using Eq. (9) was relatively similar to observed ice thickness (Fig. 5, red line). The result of the 1-D model suggested that the high snow thermal

conductivity in the CFSR would be a source of error in predicting sea ice growth.

Although the initialization and snow parameterization in the improved model was successful in matching sea ice thickness to observed values, the rapid sea ice growth in the CFSR during September and October (Fig. 4a) was still unexpected. The same issues have been shown by Johnson et al. (2012). Collow et al. (2015) reported that improved initial sea ice thickness and atmospheric model physics (e.g. maritime clouds) reproduced the seasonal cycle of sea ice thickness well. Sea–ice dynamic processes such as ridging may be another influencing factor. IMBs measure the thermodynamic growth of level ice (Perovich et al. 2017), while the sea ice thickness in the CFSR can be increased by both thermodynamic and dynamic processes. Because the ice growth rate from the 1-D thermodynamic model without a dynamic process was accurately reproduced if an adequate value of snow thermal conductivity was applied (red line in Fig. 5), the error of thermal ice growth in the CFSR (e.g. blue line in Fig. 5) would be amplified when a dynamic process contributed to thickening of the sea ice by rafting and ridging.

3.3 Sensitivity of ice growth rate to enhanced snow depth

Accumulated snow on sea ice in autumn is important to thermal transfer through the ice column during winter and spring. The overestimation of ice thickness in the CFSR caused difficulty in estimating the sea ice growth rate. For that reason, the 1-D thermodynamic model was used to understand the impact of changes in snow depth and surface forcing of ice growth from September through the following May (Fig. 6). We focused on the relationship between enhanced snow depth in autumn and ice growth rate during winter and spring over the northern Chukchi Sea (74–77°N, 170–200°E) where increase

Table 2 Snow depth in November averaged over 74°–77°N, 170°–200°E and sea ice thickness on 16 September for 1979–1983 and 2009–2013. Values are from the CFSR

	Period 1: 1979–1983	Period 2: 2009–2013
Average sea ice thickness on 16 September by period (cm)	189	59
Average snow depth in November by period (cm)	18	26

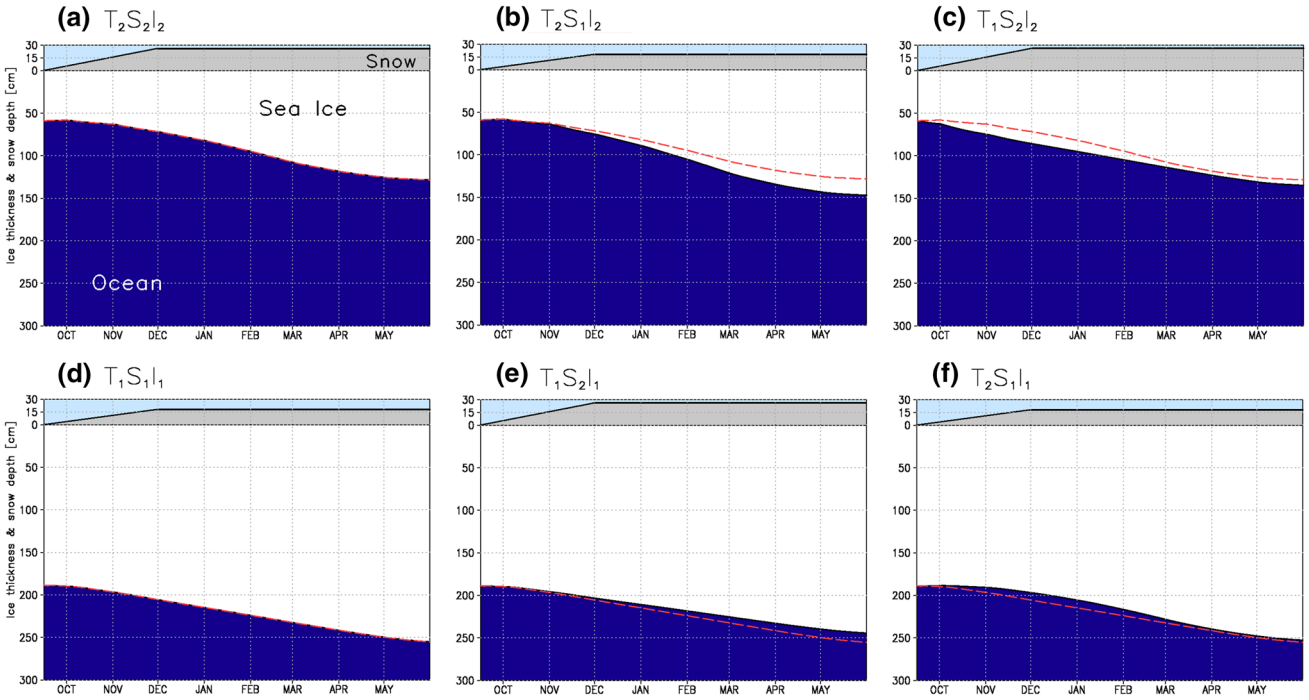

Fig. 6 Modeled sea ice thickness over the Beaufort Sea using different snow and temperature parameterizations for **a** $T_2S_2I_2$, **b** $T_2S_1I_2$, **c** $T_1S_2I_2$, **d** $T_1S_1I_1$, **e** $T_1S_2I_1$ and **f** $T_2S_1I_1$. The six experiments were done with different combinations initializations for surface heat budgets and air temperature (T), snow depth (S), and ice thickness (I) (Table 3), where the subscripts of each experiment indicate the representative period (1: 1979–1983 or 2: 2009–2013) for each parameter (T, S, and I)

in snow depth was found during 1979 and 2013 (Fig. 3d). To investigate the impact of recent changes in snow depth on sea ice growth, we selected two periods (1979–1983 and 2009–2013) under cold and warm Arctic conditions. Table 2 shows initialized sea ice thickness on 16 September and average snow depth in November for each period. The experiments were initialized with several sea ice layers and snow depths to better understand the impact of snow depth variation on sea ice growth. According to Maykut and Untersteiner (1971), changes in snow depth were negligible from December through May because of too little snowfall. The IMB buoy data showed no significant change of monthly snow depth from December through April, indicating that this depth depends on the depth of snow in November. Based on these results, snow depths in the experiments were assumed to have linear accumulations of 18 cm and 26 cm between 16 September and 31 November for 1979–1983 and 2009–2013, respectively (Fig. 6). Surface heat forcing and temperature were derived from monthly mean data using the CFSR reanalysis. We applied the parameterization of Eq. (9) to snow thermal conductivity in all experiments.

Six experiments ($T_2S_2I_2$, $T_2S_1I_2$, $T_1S_2I_2$, $T_1S_1I_1$, $T_1S_2I_1$, and $T_2S_1I_1$) were done with different combinations of initializations for surface heat budgets and air temperature (T), snow depth (S), and ice thickness (I) (Table 3), where the subscripts of each experiment indicate the representative decade (1: 1979–1983 or 2: 2009–2013) for each parameter (T, S, and I). The difference in ice thickness between $T_2S_2I_2$ (Fig. 6a) and $T_2S_1I_2$ (Fig. 6b) can be attributed to the impact of recent increased snow depth on the thermodynamic ice growth. The value was 20 cm (Table 3), indicating that the ice growth was reduced by 30% when the snow depth was increased from 18 cm (Fig. 6b) to 26 cm (Fig. 6a) over the Chukchi Sea. Therefore, the recent enhanced snow depth prevented ice growth during winter and spring, as expected. Comparing $T_2S_2I_2$ (Fig. 6a) and $T_1S_2I_2$ (Fig. 6c), the impact of Arctic warming during autumn and winter on the sea ice growth (7cm: 10%) was smaller than that of the snow depth anomaly (20 cm) although the sea ice grew quickly during November because of stronger cooling (Fig. 6c). Thus, the role of increased snow depth is relatively important for the recent thinning of sea ice, in particular for thin ice, compared with the role of atmospheric warming.

The growth rate of thick sea ice was reduced by enhanced snow depth (Fig. 6d, e); however, the impact of change in snow depth on ice growth was limited to 11 cm. Applying the surface temperature and surface heat budget for 2009–2013 ($T_2S_1I_1$), the amount of ice growth was nearly the same as that for $T_1S_1I_1$ (Fig. 6d, f). Overall, the increase in snow depth on the sea ice prevented effective seasonal growth in thin ice rather than thick ice.

3.4 Comparison between CFSR and satellite data sets

Based on spatial snow depth measurements at 10-meter intervals, Warren et al. (1999) reported that the values of snow depth significantly deviated among the measurement points, implying that snow depth as well as sea ice thickness observed by IMB would have large errors due to the reduced spatial representativeness of these parameters. To evaluate the measurement of changes of the CFSR snow depth and sea ice thickness at a regional scale, we compared the CFSR and data from ICESat and CryoSat-2. Figure 7 shows the seasonal cycles of monthly

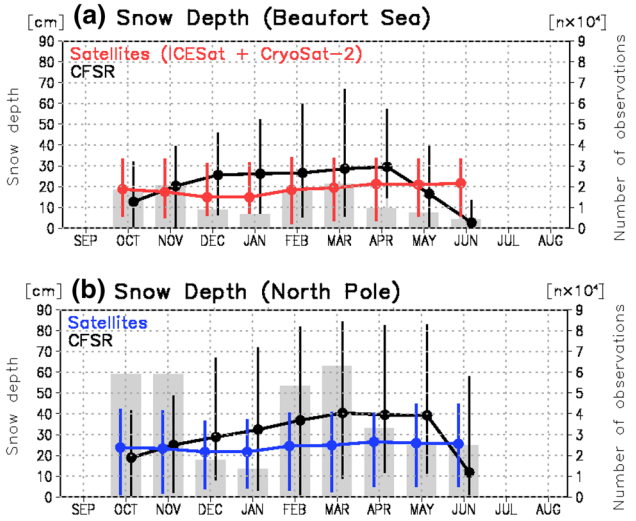

Fig. 7 **a** Monthly average snow depth on sea ice from CFSR (*black*) and Satellites (*red*) over the Beaufort Sea during 2003–2013. *Vertical lines* indicate ranges of snow depth in each month. *Gray bars* show number of observations. **b** Same as (**a**), but for North Pole

Table 3 The input and output data for the 1-D sea-ice model

Model run	$T_2S_2I_2$	$T_2S_1I_2$	$T_1S_2I_2$	$T_1S_1I_1$	$T_1S_2I_1$	$T_2S_1I_1$
Snow depth in November	26	18	26	18	26	18
Initialized ice thickness on 16 September	59	59	59	189	189	189
Surface forcing	2009–2013	2009–2013	1979–1983	1979–1983	1979–1983	2009–2013
Sea ice growth from December to May (cm)	69	89	76	66	55	64

averaged snow depth over the Beaufort Sea (70°–80°N, 170°–240°E) and the North Pole (north of 80°N). Red and blue lines show monthly averaged snow depth obtained by satellites for the Beaufort Sea (orange dotted line in Fig. 1) and the North Pole (purple dotted line in Fig. 1). Black lines denoted average CFSR snow depth for each area. In the Beaufort Sea, the CFSR had positive snow depth biases during November and April, and had negative snow depth biases during May and June because of early snow melting (Fig. 7a). In the North Pole, there were positive snow depth biases during November and May (Fig. 7b). The seasonal cycles of snow depth biases between the CFSR and satellite observations show the same trends as those in Fig. 2a, b, whereas the CFSR had a negative bias during October in the Beaufort Sea (Fig. 2a).

The same evaluation was done for sea ice thickness (Fig. 8). The differences in sea ice thickness between the CFSR and satellite observations became larger from November through January in the Beaufort Sea. These differences remained constant during February and April, then gradually decreased during May and June. These differences were larger than those in Fig. 4a because the satellite ice thicknesses were thinner than IMBs ice thicknesses. The averaged satellite ice thicknesses included relatively thinner first-year ice over the Beaufort Sea, which would cause quite large biases between the CFSR and satellite results. In contrast, in the North Pole, there were relatively small biases in ice thickness compared with Fig. 4b. The averaged satellite sea ice thicknesses, including relatively thicker MYI over the north part of Greenland, were thicker

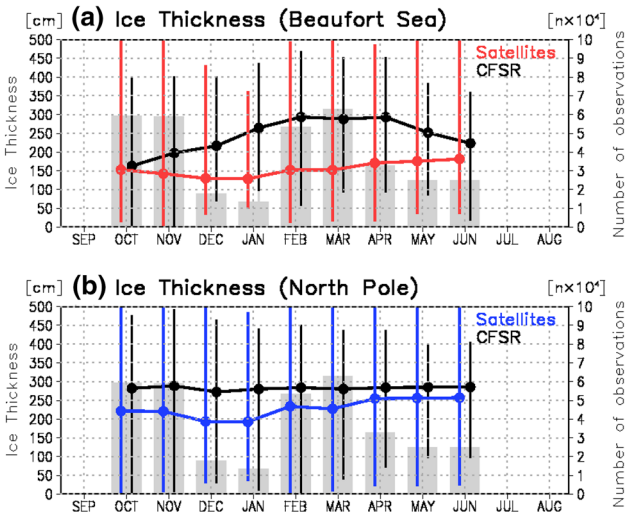

Fig. 8 **a** Monthly average sea ice thickness from CFSR (*black*) and Satellites (*red*) over the Beaufort Sea during 2003–2013. *Vertical lines* indicate ranges of sea ice thickness in each month. *Gray bars* show number of observations. **b** Same as (**a**), but for North Pole

than those in IMBs. However, the biases between the CFSR and satellite observations supported the results of the comparison between IMB and the CFSR.

4 Conclusions

The objectives of the present study were to estimate the accuracy of snow depth and ice thickness in the CFSR and to study the effect of changes in snow depth on Arctic sea ice and causes of that change using the CFSR. Comparison of the CFSR with IMB buoy data showed that simulated snow depth was in good agreement with in situ snow depth during November. However, there was earlier snow melt in the CFSR simulations in May compared with IMB buoys as well as satellite products, suggesting that the reanalysis helped to understand the snow depth distribution on Arctic sea ice during early winter.

From 1979 to 2013, snow depth increased more than 2 cm per decade over the northern Chukchi Sea during November. This was induced by an increase in both robust synoptic activity and strong upward turbulent heat flux because of sea ice retreat (Kurita 2011). Several studies have suggested that decreases in snow depth during March and April are generated by the delayed onset of sea ice freeze-up during autumn (Kurtz and Farrell 2011; Kwok et al. 2011; Webster et al. 2014). Comparison between IMB buoy and Soviet drifting station data suggested that the snow accumulation rate has not changed (Webster et al. 2014). Differences in the location of the buoys and drifting stations should not cause significant changes in snow accumulation. Our study showed that a significant positive trend in precipitation contributed to increased snow depth during November, when sea ice freeze-up began. This implied that the impact of delayed sea ice freeze-up on snow depth change was limited over the Chukchi Sea.

The error in dynamic thickening processes such as rafting and ridging in the CFSR might cause a bias in estimating the sea ice thickness. However, experiments with a 1-D thermodynamic model showed that an unrealistically high snow thermal conductivity in the CFSR led to an overestimation of ice growth. The positive sea ice bias because of high snow thermal conductivity caused further positive ice thickness bias when ridge ice occurred. Using an adequate snow thermal conductivity in the model, we estimated the influence of enhanced snow on ice growth through the thermal insulating effect. The modeling experiments suggested that the increase in snow depth was one of the major factors that reduced sea ice growth. For 2003–2008, the ICESat showed that sea ice thickness declined by 64% over the Chukchi Cap and 50% over the Beaufort Sea, relative to observed ice thickness during 1978–2000 (Kwok and Rothrock 2009). The thinner sea ice associated with sea ice

melt during summer was sensitive to snow depth variation over the Beaufort and Chukchi Seas, resulting in a reduced recovery of sea ice and early exposure of open water.

Anomalous surface heating associated with early snowmelt on land alters atmospheric circulation over the Arctic (Matsumura and Yamazaki 2012). The latter study indicated that the atmospheric response to changes in the length of snow cover reduced summer sea ice concentration along the Siberian coast. However, an increase in surface albedo associated with increased snow cover was not found over the Beaufort and Barents Seas. In contrast, the albedo trend during July was negative in the Pacific sector of the Arctic. Snowfall has decreased because of warming of the lower atmosphere, increasing surface melt ponds in July (Screen and Simmonds 2012). Therefore, sensitivity experiments must be performed that implement changes in snow density and surface albedo associated with seasonal variability in the near future.

Acknowledgements This work was supported by the Arctic Challenge for Sustainability (ArCS) project and a Grant-in-Aid for Scientific Research (KAKENHI(DC1)2510583 and KAKENHI(A)24241009) from the Ministry of Education, Culture, Sports, Science and Technology, Japan. Processing of the CryoSat-2 (PARAMETER) was funded by the German Ministry of Economics Affairs and Energy (Grant: 50EE1008). We thank two anonymous reviewers for very helpful comments. We also thank H. Enomoto, M. Shiobara, Y. Tachibana, J. Ukita for helpful discussions and comments.

Appendix

In this study, we used the snow depth and sea ice thickness calculated from freeboard and ice thickness by satellites (ICESat and CryoSat-2). The details of calculation are described in Kwok and Cunningham (2008). Because the observed freeboard and ice thickness include serious errors due to radar signal noise (Wingham et al. 2006) and inadequate sampling (Warren et al. 1999), the comparison between a CFSR grid and the closest ICESat pixel may sometimes cause unexpected errors. These errors can be reduced by averaging a group of pixels. First, all freeboard and ice thickness measurements which are close to each center of a CFSR grid within $0.25° \times 0.25°$ are collected. In the ICESat data set, this equates to more than 100 samples which are enough to reduce radar noise error. In the CryoSat-2 data set, such a procedure was not applied because the product has been already averaged and re-gridded with a resolution of 25 km when the number of samples was satisfied (Ricker et al. 2014). Second, if the satellite data was not available in the CFSR grid, we did not use that CFSR grid for the comparison. Third, using comparable CFSR and satellite datasets, monthly averaged snow depth and sea ice thickness for each region (Fig. 1) in each year were calculated.

References

Blazey BA, Holland MM, Hunke EC (2013) Arctic Ocean sea ice snow depth evaluation and bias sensitivity in CCSM. Cryosphere 7:1495–1532

Collow T W, Wang W, Kumar A, Zhang J (2015) Improving Arctic sea ice prediction using PIOMAS initial sea ice thickness in a coupled ocean-atmosphere model. Mon Wea Rev 143:4618–4630. doi:10.1175/MWR-D-15-0097.1.

Comiso JC (2012) Large decadal decline of the Arctic multilayer ice cover. J Clim 25:1176–1193

Deser C, Tomas R, Alexander M, Lawrence D (2010) The seasonal atmospheric response to projected Arctic sea ice loss in the late twenty-first century. J Clim 23:333–351. doi:10.1175/2009JCLI3053.1

Hezel PJ, Zhang X, Bitz CM, Kelly BP, Massonner F (2012) Projected decline in spring snow depth on Arctic sea ice caused by progressively later autumn open ocean freeze-up this century. Geophys Res Lett 39:L17505. doi:10.1029/2012GL052794

Inoue J, Hori ME, Tachibana Y, Kikuchi T (2010) A polar low embedded in a blocking high over the Pacific Arctic. Geophys Res Lett 37:L14808. Doi:10.1029/2010GL043946

Inoue J, Hori ME, Takaya K (2012) The role of Barents Sea ice in the wintertime cyclone track and emergence of a warm-Arctic cold-Siberian anomaly. J Clim 25:2561–2568

Johnson M, Coauthors (2012) Evaluation of Arctic sea ice thickness simulated by Arctic Ocean Model Intercomparison Project models. J Geophys Res 117:C00D13. doi:10.1029/2011JC007257

Krasting JP, Broccoli AJ, Dixon KW, Lanzante JR (2013) Future change in Northern Hemisphere snowfall. J Clim 26:7813–7828

Kurita N (2011) Origin of Arctic water vapor during the ice-growth season. Geophys Res Lett 38:L02709

Kurtz NT, Farrell SL (2011) Large-scale survey of snow depth on Arctic sea ice from Operation IceBridge. Geophys Res Lett 38:L20505. doi:10.1029/2011GL049216

Kwok R, Cunningham GF (2008) ICESat over Arctic sea ice: Estimation of snow depth and ice thickness. J Geophys Res 113:C08010. doi:10.1029/2008JC004753

Kwok R, Rothrock DAF (2009) Decline in Arctic sea ice thickness from submarine and ICESat records 1958–2008. Geophys Res Lett 36:L15501. doi:10.1029/2009GL039035

Kwok R, Zwally HJ, Yi D (2004) ICESat observations of Arctic sea ice: A first look. Geophys Res Lett 31:L16401. doi:10.1029/2004GL020309

Kwok R, Panzer B, Leuschen C, Pang S, Markus T, Holt B, Gogineni S (2011) Airborne surveys of snow depth over Arctic sea ice. J Geophys Res 116:C11018. doi:10.1029/2011JC007371

Laxon SW, Giles KA, Ridout AL, Wingham DJ, Willatt R, Cullen R, Kwok R, Schweiger A, Zhang J, Haas C, Hendricks S, Krishfield R, Kurtz N, Farrell S, Davidson M (2013) CryoSat-2 estimates of Arctic sea ice thickness and volume. Geophys Res Lett 40:732–737. doi:10.1002/grl.50193

Lecomte O, Fichefet T, Vancoppenolle M, Domine F, Massonnet F, Mathiot P, Morin S, Barriat PY (2013) On the formulation of snow thermal conductivity in large-scale sea ice models. J Adv Model Earth Syst 5:542–557. doi:10.1002/jame.20039

Lindsay R, Wensnahan M, Schweiger A, Zhang J (2014) Evaluation of seven different atmospheric reanalysis products in the Arctic. J Clim 27:2588–2606

Liu J, Curry JA, Wang H, Song M, Horton RM (2012) Impact of declining Arctic sea ice on winter snowfall. P Natl A Sci 109:4074–4079

Markus T, Stroeve JC, Miller J (2009) Recent change in Arctic sea ice melt onset, freezeup, and melt season length. J Geophys Res 114:C12024. doi:10.1029/2009JC005436

Maslanik JA, Fowler C, Stroeve J, Drobot S, Zwally J, Yi D, Emery W (2007) A younger, thinner arctic ice cover: Increased potential for rapid, extensive sea-ice loss. Geophys Res Lett 34:L24501. doi:10.1029/2007GL032043

Maslanik J, Stroeve J, Fowler C, Emery W (2011) Distribution and trends in Arctic sea ice age through spring 2011. Geophys Res Lett 38:L13502. doi:10.1029/2011GL047735

Matsumura S, Yamazaki K (2012) Eurasian subarctic summer climate in response to anomalous snow cover. J Clim 25:1305–1317

Matsumura S, Yamazaki K, Tokioka T (2010) Summertime land-atmosphere interactions in response to anomalous springtime snow cover in northern Eurasia. J Geophys Res 115:D20107. doi :10.1029/2009JD-12342

Maykut GA, Untersteiner N (1971) Some results from a time-dependent thermodynamic model of sea ice. J Geophys Res 76(6):1550–1575

Perovich DK, Light B, Eicken H, Jones KF, Runciman K, Nghiem SV (2007) Increasing solar heating of the Arctic Ocean and adjacent seas, 1979–2005: attribution and role in the ice-albedo feedback. Geophys Res Lett 34:L19505. doi:10.1029/2007GL031480

Perovich DK, Richter-Menge JA, Elder B, Claffey K, Polashenski C (2017) Observing and understanding climate change: monitoring the mass balance, motion, and thickness of Arctic sea ice. Cold Regions Research and Engineering Laboratory. http://www.imb-crrel-dartmouth.org/imb.crrel. Accessed 25 Jan 2017

Riche F, Schneebeli M (2013) Thermal conductivity of snow measured by three independent methods and anisotropy considerations. Cryosphere 7:217–227

Ricker R, Hendricks S, Helm V, Skourup H, Davidson M (2014) Sensitivity of CryoSat-2 Arctic sea-ice freeboard and thickness on radar-waveform interpretation. Cryosphere 8:1607–1622. doi:10.5194/tc-8-1607-2014

Saha S, Coauthors (2010) The NCEP climate forecast system reanalysis. Bull Am Meteorol Soc 91:1015–1057. doi:10.1175/2010BAMS3001.1

Saha S, Coauthors (2014) The NCEP climate forecast system version 2. J Clim 27:2185–2208

Sato K, Inoue J, Watanabe M (2014) Influence of the Gulf Stream on the Barents Sea ice retreat and Eurasian coldness during early winter. Env Res Lett 9:084009. doi:10.1088/1748-9326/9/8/084009

Screen JA, Simmonds I (2012) Declining summer snowfall in the. Arctic: causes impacts feedbacks Clim Dyn 38:2243–2256. doi:10.1007/s00382-011-1105-2

Serreze MC, Barrett AP, Stroeve J (2012) Recent changes in tropospheric water vapor over the Arctic as assessed from radiosonde and atmospheric reanalyses. J Geophys Res 117:D10104. doi:10.1029/2011JC017421

Steele M, Zhang J, Ermold W (2010) Mechanisms of summertime upper Arctic Ocean warming and the effect on sea ice melt. J Geophys Res 115:C11004. doi:10.1029/2009JC005849

Stroeve JC, Serreze MC, Barrett A (2011) Attribution of recent change in autumn cyclone associated precipitation in the Arctic. Tellus 63A:653–663

Stroeve JC, Kattsov V, Barrett A, Serreze M, Pavlova T, Hollamd M, Meier WN (2012) Trends in Arctic sea ice extent from CMIP5, CMIP3 and observations. Geophys Res Lett 39:L16502. doi:10.1029/2012GL052676

Sturm M, Holmgren J, König M, Morris K (1997) The thermal conductivity of seasonal snow. J Glaciol 43:26–41

Sturm M, Perovich DK, Holmgren J (2002) Thermal conductivity and heat transfer through the snow on the ice of the Beaufort Sea. J Geophys Res 107(C21):8043. doi:10.1029/2000JC000409

Warren SG, Rigor GI, Untersteiner N, Radionov VF, Bryazgin NN, Aleksandrov I, Colony R (1999) Snow depth on Arctic sea ice. J Clim 12:1814–1829

Webster MA, Rigor IG, Nghiem SV, Kurtz TN, Farrell SL, Perovich DK, Sturm M (2014) Interdecadal change in snow depth on Arctic sea ice. J Geophys Res 119:5395–5406. doi:10.1002/2014JC009985

Wingham DJ, Coauthors (2006) CryoSat: A mission to determine the fluctuations in Earth's land and marine ice fields. Adv Space Res 37:841–871

Winton M (1999) A reformulated three-layer sea ice model. J Atmos Ocean Technol 17:525–531

Yen Y (1981) Review of thermal properties of snow, ice and sea ice. CRREL Report 81–10